Mol. Cryst. Liq. Cryst., Vol. 545: pp. 3/[1227]–21/[1245], 2011

ISSN: 1542-1406 print/1563-5287 online
DOI: 10.1080/15421406.2011.571966

Taylor & Francis
Taylor & Francis Group

Towards Reconfigurable Optical Metamaterials: Colloidal Nanoparticle Self-Assembly and Self-Alignment in Liquid Crystals

DENNIS F. GARDNER, JULIAN S. EVANS, AND IVAN I. SMALYUKH

Department of Physics, Renewable and Sustainable Energy Institute, and Liquid Crystal Materials Research Center, University of Colorado, Boulder, CO, USA

We explore the nanoscale colloidal self-assembly and self-alignment in liquid crystals. We use model particles with controlled shapes and sizes, including quantum dots and rods and metal nanoparticles in the form of spheres, rods, and polygonal platelets. To study these composites on the scales ranging from nanometers to millimeters and to motivate their use in metamaterial fabrication, we utilize optical microscopies, freeze-fracture transmission electron microscopy, and cryogenic transmission electron microscopy. We discuss the long-range alignment and assembly of anisotropic nanoparticles imposed by the orientational elasticity of liquid crystals, showing that these composites provide a powerful platform for self-assembly of metamaterials.

Keywords Colloids; liquid crystal; metamaterial; nanoparticle; self-assembly; topological defect

1. Introduction

Optical metamaterials are a new class of man-made materials with the potential for a broad range of breathtaking applications that range from nanoscale diffraction-unlimited optical imaging with "perfect" lenses to invisibility cloaking [1–25]. They are composed of ordered arrays of predesigned structural units different from those in the conventional matter and allow for the engineering of unprecedented material properties. These ordered structures of predesigned anisotropic nanoparticles play the role of "building blocks" similar to that of molecules and atoms in conventional condensed matter systems [1–25]. Metamaterials allow for engineering of unprecedented physical properties not encountered in naturally occurring materials, such as negative refraction of light [1,2]. However, for these applications to come within reach, large-scale fabrication approaches are needed [5,15].

Address correspondence to Ivan I. Smalyukh, Department of Physics, Renewable and Sustainable Energy Institute, and Liquid Crystal Materials Research Center, University of Colorado, Boulder, CO 80309, USA. Tel.: +303-492-7277; Fax: +303-492-2998; E-mail: ivan.smalyukh@colorado.edu

Hybrid nanostructured materials based on nanoparticles and liquid crystals (LCs) are a class of composites poised to revolutionize scientific instruments, technologies, and devices, and may enable self-assembly-based approaches for fabrication of metamaterials [15]. LCs may enable reconfigurable and switchable self-assembly of dispersed nanoparticles directed by the nanoscale molecular ordering in these anisotropic fluids with a broad range of mesomorphic phases. Control of the colloidal and molecular structural organization and ensuing composite properties may be achieved by using intrinsic liquid crystalline self-assembly and re-assembly into various mesomorphic phases (including phases that have not been encountered previously), applying external electric, magnetic, mechanical, and optical fields, varying temperature, and changing surface treatment at the nanostructured solid-LC interfaces [31]. However, the nanoscale interactions between colloidal nanoinclusions in LC media remain poorly understood. There is a need to explore the fundamental organizing principles of this type of LC-directed self-assembly arising from the controlled structuring of switchable liquid crystalline order and nanoparticles of various shapes and chemical composition.

In this article, we discuss the nanoscale colloidal self-assembly and self-alignment in LCs probed for a variety of model particles with controlled shapes and sizes. External magnetic and electric fields and shearing allow for alignment and realignment of the LC matrix with the ensuing reconfigurable long-range orientational order of the dispersed nanoparticles that can be kept dispersed or made to self-organize into structures such as chains and periodic lattices. The device-scale bulk nanoparticle self-alignment and self-assembly may enable optical metamaterial mass production and control of their properties arising from combining the switchable nanoscale structure of LCs and the so-called Surface Plasmon Resonance (SPR) properties of the plasmonic nanoparticles [15]. Potential applications of these man-made artificial materials include ''perfect'' lenses for imaging with sub-wavelength resolution, better optical tweezers, wide-angle non-mechanical beam steering devices, novel band gap materials, high-density optical data storage, stealth technology (i.e., invisible warfare), and many other applications [1–33]. Metamaterials also provide an incredible range of untouched fundamental science problems and engineering challenges which greatly stimulate the development of novel nanoparticle synthesis approaches, techniques for nanoparticle dispersion and assembly, etc. [34–49].

This article will show that the LC colloidal nanoparticle dispersions provide a powerful platform for self-assembly-based tunable optical metamaterial fabrication and may allow their potential applications to come within reach. We provide the motivation and a brief introduction to the fundamental aspects of metamaterials in the next section 2 and then proceed with the description of the used materials and experimental techniques in the section 3. The main results are described in section 4, followed by a brief discussion (section 5), and concluding remarks (section 6).

2. *Structure and Potential Applications of Metamaterials*

In terms of resolution, optical imaging of long-range molecular orientation patterns had only incremental improvements over a century of its use, even though it is one of the most important and frequently used techniques in the LC research. Novel approaches of imaging of structural self-assembly in LCs with improved resolution

are needed to further the collective understanding of these media on the nanoscale. Therefore, motivating this work with the current state-of-the-art of nanoscale LC imaging is a convincing way of presenting the importance and the need for the development of optical metamaterials. Figure 1 shows nanoscale images of a chromonic lyotropic LC obtained by a cryogenic transmission electron microscope (TEM), a powerful nanoscale imaging technique that is rarely available to researchers. Because of the need to freeze the samples and a number of other limiting factors, this technique is incapable of revealing the dynamics of the nematic and columnar hexagonal ordering of the constituent molecular stacks. Despite of the recent interest in the lyotropic chromonic LCs, they remain poorly understood, and even the types of molecular organization into chromonic stacks still need to be clarified for some of the most common materials. Cryogenic TEM images in Figure 1 show that molecular stacking in nematic and columnar hexagonal phases is qualitatively different. Nematic-phase stacks possess multiple kinks and can relatively easily bend or branch

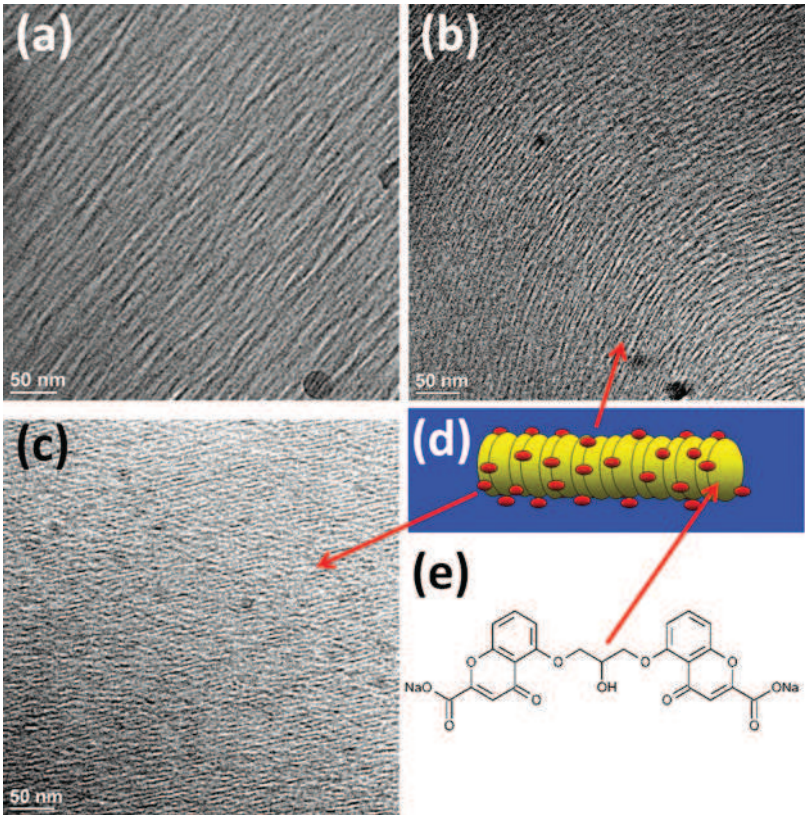

Figure 1. Nanoscale imaging of a chromonic lyotropic LC by means of the Cryogenic Transmission Electron Microscopy. a–c) Cryogenic TEM images obtained for an aqueous solution of cromolyn sodium in (a,b) nematic and (c) columnar hexagonal phases. d) a schematic representation of a columnar stack that is a building block of both columnar hexagonal and nematic phases of the chromonic lyotropic LC. e) Chemical structure of cromolyn sodium used to obtain the studied LC in its aqueous solutions (section 3.2). (Figure appears in color online.)

into multiple stacks (Fig. 1a,b). Columnar stacks in the hexagonal phase (Fig. 1c) are much more regularly structured and highly ordered as compared to those in the nematic phase. These images give the average length of the molecular aggregates of molecules of Cromolyn Sodium which is 50–100 nm in the nematic phase and even longer (hundreds of nanometers) in the columnar hexagonal phase as well as high values (0.8–0.95) of the orientational order parameter in these phases [50]. However, cryogenic TEM fails to reveal the temporal evolution of the molecular stacks and how they change and rearrange during phase transitions, switching by external fields, etc. On the other hand, noninvasive diffraction-limited optical imaging in different modes [51–57] lacks the nanoscale resolution needed to address this problem. Although there have been recent developments in optical imaging that allow overcoming the diffraction limit [58–60], their use is typically restricted to very specific chromophores and would not be easily applicable for imaging of soft matter systems such as chromonic LCs.

Recently, a bulk of theoretical and experimental research showed the feasibility of diffraction-unlimited optical imaging by use of simple optical elements based on metamaterials with a negative index of refraction. Theoretical works of Veselago [1] and Pendry [2], followed by numerous theoretical and experimental papers [3–33], have demonstrated that the diffraction limit of conventional lenses (Fig. 2a) is not a limiting factor for the focusing of light by a lens made of a flat slab of metamaterial with a negative index of refraction (Fig. 2b), often referred to as a ''super-lens'' or

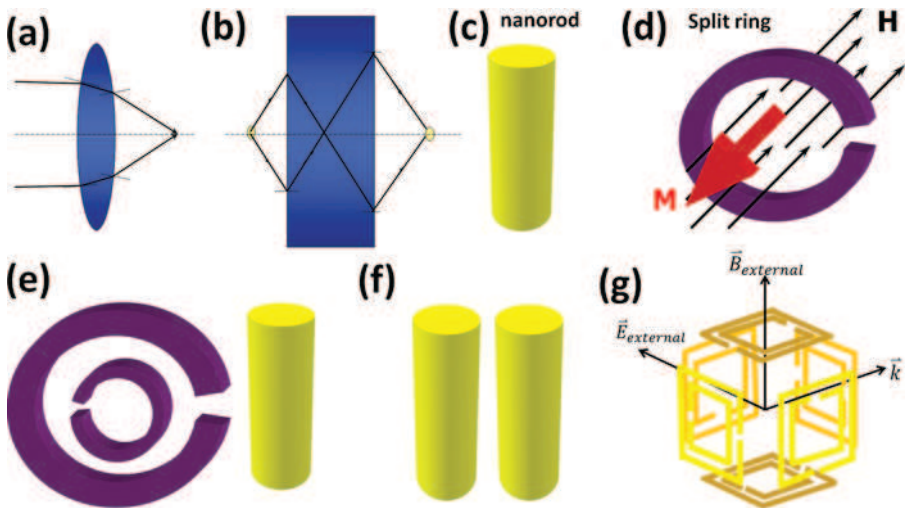

Figure 2. Motivation for the development of optical metamaterials and common designs of their structural units. a,b) comparison of light focusing by lenses made of a) conventional materials and b) a flat slab of the metamaterial with a negative index of refraction. Structural elements of metamaterials: c) plasmonic nanorods for negative electric response, d) split nanorings for negative magnetic resonance, e) double split nanorings paired with nanorods to provide negative electric and magnetic response, f) coupled nanorods also capable of providing negative electric and magnetic response in certain conditions, g) a unit cell of a three-dimensional optical metamaterial composed of double split rings [1–33]. (Figure appears in color online.)

a ''perfect lens.'' Improved resolution of the negative-index super-lens is due to the transmission of the evanescent surface waves, which (unlike in the case of conventional lenses) are not lost. Being first considered theoretically over four decades ago by Veselago [1], metamaterials (also called ''left-handed materials'') have never been encountered in nature or fabricated until the theoretical work of Pendry provided important physical insights into how these unusual materials can be realized [2].

Metamaterials are composed of structural units much smaller than the wavelength of incident light, so they appear homogeneous to the waves. To obtain metamaterials with a negative refractive index, one has to achieve simultaneous negative electric and magnetic response in the artificial nanofabricated composite material. At optical frequencies close to the SPR peaks, the electric response can be negative. Therefore, achieving negative electric response (dielectric constant) is relatively easy when using metal nanoparticles, because they show SPR peaks dependent on material composition and shape. For example, gold nanospheres have one SPR peak at $\sim$525 nm and silver nanospheres exhibit SPR at $\sim$420 nm, while metal nanorods and particles of more complex shapes have more than one SPR peak with the spectral locations dependent on the shapes and aspect ratios of these nanoparticles. For nanorods, there are two resonance modes, transverse & longitudinal, both of which can be located within the visible spectral range (Fig. 2c). To have different SPR peaks within the visible spectrum, one typically needs to use nanoparticles with fairly small (1.5–3) aspect ratios as the larger the aspect ratio, the longer is the wavelength of the longitudinal peak and the wavelength of the transverse peak is fixed and similar to that of spheres. Achieving strong negative magnetic response at optical frequencies, however, is more difficult than obtaining negative electrical response (considered being impossible until about a decade ago). This was part of the reason why Veselago's left-handed materials have not attracted much attention in the scientific and engineering communities until recently. Pendry proposed that split-ring resonators could produce a strong negative magnetic response (Fig. 2d) [2], inspiring a bulk of experimental and theoretical research that led to confirmation of his theoretical predictions and to a ''metamaterial rush'' in the optics and materials research communities [2–33]. The predesigned structural units of metamaterials can be built out of nanoparticles designed to provide negative electric and magnetic response. Popular metamaterial designs involve pairs of double-split rings and rods (Fig. 2e), coupled rods (Fig. 2f), and three-dimensional structures composed of multiple double-split rings (Fig. 2g) [2–33].

Various nanofabrication approaches have been successfully utilized to produce nanoscale structures exhibiting metamaterial properties. Metamaterials working in the infrared and visible spectral ranges have been recently proposed and realized, with the so-called ''fishnet metamaterials'' being perhaps the most successful example. However, as already mentioned in the introduction, for practical applications of these artificial materials to come within reach, self-assembly-based approaches for mass production of large-scale three-dimensional metamaterials need to be developed [5,15,33]. LCs with the intrinsic long-range orientational and partial positional ordering can provide several critical components in this effort, including self-assembly and self-alignment of nanoparticles, their spatial self-positioning and chiral arrangement, as well as optical, electric, magnetic, thermal and other means of control and switching applied to LC-incorporated particles of pre-designed shapes and composition.

3. Materials and Experimental Techniques

3.1. *Synthesis of Gold Nanoparticles*

Although gold nanoparticles have been used in red stained glass in cathedrals for centuries and have been studied extensively starting from the works by Faraday, their potential use in metamaterials requires a precise control of particle shapes and their spatial structuring on length scales much smaller than the wavelength of visible light. This sets new fundamental research and engineering challenges from the standpoint of their synthesis, dispersion, and controlled structural organization. The synthesis of colloidal gold nanoparticles typically occurs through the reduction of gold cations in the presence of a certain capping agent. The size and shape of the nanoparticles are determined by the kinetics of nucleation, the ratio of gold and capping agent, and the stabilization of different crystallographic faces by the capping agents [61]. To produce spherical particles, fast reduction with no preferential surface stabilization is ideal. For example, in the Brust-Schiffrin method, chloroauric acid is complexed with tetraoctylammonium bromide (TOAB) and toluene to enter the organic phase [62]. It is then reduced by sodium borohydride in the presence of excess thiol to produce 2 nm spheres (Fig. 3a). If no thiol is added, TOAB stabilizes the formation of 20 nm spheres (Fig. 3b).

The growth of non-spherical nanoparticles requires slower reduction and preferential selection of crystal facets. One of the best known examples of synthesis of non-spherical metal nanoparticles is the synthesis of nanorods capped by cetyl trimethylammonium bromide (CTAB) [63,64]. In the synthesis procedure, spherical seeds are produced by reducing chloroauric acid with sodium borohydride in the presence of sodium citrate or CTAB. These spherical seeds are then transferred to

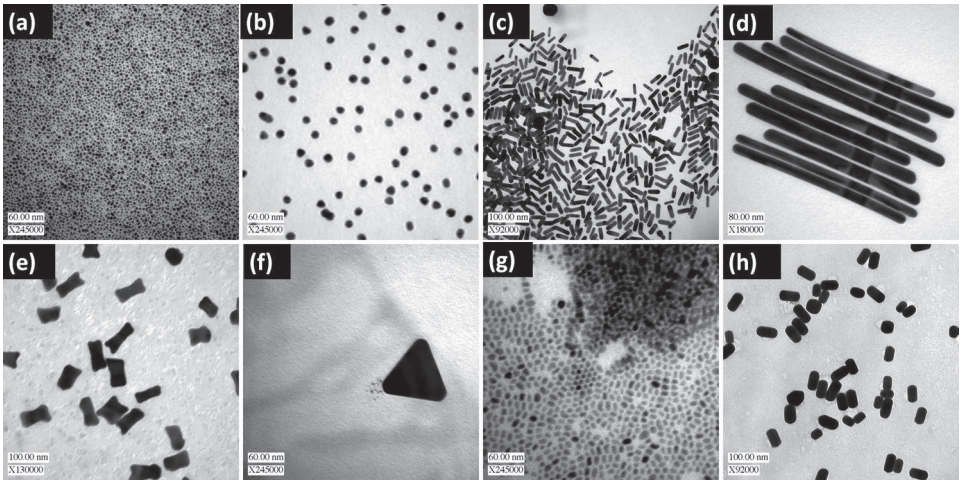

Figure 3. Examples of nanoparticles of different material composition, shapes, and sizes. a) Gold nanospheres of 2–3 nm in diameter. b) gold spheres of 20 nm in diameter. c) CTAB capped gold nanorods with an aspect ratio of about 3. d) CTAB capped gold nanorods with aspect ratios ranging from 15 to 20. e) dog-bone-shaped gold nanoparticles. f) PVP capped silver triangle synthesized by photoreduction. g) CdSe quantum rods with aspect ratio of about 2. h) short gold nanorods obtained from NanoPartz.

a growth solution with more CTAB, chloroauric acid, and ascorbic acid that produces a mild reduction on the $<110>$ facets of the seed particles [65] (Fig. 3c,d). If the ascorbic acid is too active, then the ends can get overgrown producing anisotropic nanoparticles with shapes resembling "dog bones" [66] (Fig. 3e). Triangular platelets can be synthesized using various methods such as photoreduction (Fig. 3f) [67] and biosynthesis [68]. These triangles and dog bones mentioned above are of special interest for the metamaterial applications because the SPR that they exhibit is enhanced by sharp corners. CdSe quantum dots and rods were obtained as described in ref [48,60]. and provided by P. Prasad. Gold Nsol rods were obtained from Nanopartz Inc. (Loveland, Colorado, USA).

3.2. *Nanoparticle Dispersion in LCs and Cell Preparation*

Before introducing nanoparticles into the thermotropic LC host they are first dispersed in an organic solvent. Then the particles are continuously added (2 μl at a time) to the LC while the mixture is rapidly stirred by a magnetic stir bar. The LC with the added nanoparticles is kept at an elevated temperature (above the boiling point of the used solvent) overnight to evaporate the solvent. For example, the sample is kept overnight at 80°C in the case of hexane (above its boiling point) to assure that the solvent is fully removed from the sample through evaporation. After the solvent is evaporated, the sample is vigorously stirred for three minutes using a VWR Analogue Vortex Mixer, sonicated for three minutes by a Branson 250 Sonifier, and finally sonicated for 3 minutes in a Cole Parmer 8891 ultrasonic bath to ensure that nanoparticles are well dispersed in the LC.

The dispersion of nanoparticles in lyotropic LCs is limited to nanoparticles functionalized or capped with surfactants. For example, the synthesis procedure of the gold nanorods yields CTAB-capped rods dispersed in an aqueous solution. We add more CTAB (surfactant) and benzyl alcohol (cosurfactant) to this aqueous nanorod dispersion to obtain the desired lyotropic LC phase according to the phase diagram of aqueous mixtures of surfactant CTAB and co-surfactant benzyl alcohol previously studied without adding nanoparticles [15,69,70]. For example, the LC-nanorod dispersion in the columnar hexagonal phase is prepared using a composition of 25% CTAB, 5% benzyl alcohol (both from Aldrich, used as supplied) and 70% of aqueous suspension of CTAB-capped GNRs. The nematic phase is prepared in a similar way, but consists of 25% CTAB and 75% of aqueous suspension of CTAB-capped GNRs. This preparation is typically followed by centrifugation at 3000 rpm for 10 min. The obtained LC-nanoparticle composites are sonicated in the ultrasonic bath for two hours to ensure homogeneous mixing and dispersion.

For optical microscopy observations, the LC-nanoparticle dispersions are filled into a rectangular capillary or glass cell by use of capillary action. The glass cells are typically made of a clean microscope slide and a cover slip. The microscope slide and cover slip are glued together using UV-curable glue mixed with glass spacers that set the cell gap. Typically, the substrates have no alignment layers. The cell substrates are sealed using a 5-min epoxy.

3.3. *Optical Microscopy and Spectroscopy*

Optical imaging of nanoparticle-LC composites is performed using an Olympus BX-51 upright optical polarizing microscope with a fluorescent attachment. The

dispersion quality (i.e., absence of micron-scale or larger nanoparticle aggregates) is assessed by means of the transmission-mode bright-field imaging. The phase behavior and LC alignment is studied by the same microscope in the polarizing optical imaging mode using 10×, 20×, and 50× air objectives (all from Olympus) with numerical aperture NA = 0.3–0.9 as well as a Spot 14.2 Color Mosaic Camera (from Diagnostic Instruments, Inc.). In addition, we have used an inverted microscope IX81 with a fluorescence attachment, a confocal microscopy scanning unit, and a NA = 1.4 objective (all from Olympus). The SPR extinction spectra are measured using a USB-2000 microspectrometer (Ocean Optics) mounted on the optical microscope.

3.4. *Nanoscale Imaging of Nanoparticles in Liquid Crystals*

The images of the synthesized nanoparticles, such as those shown in Figure 3, are obtained using a Philips CM10 TEM (FEI, Inc.) operating at 80kv. However, regular TEM is not appropriate for probing the structural assembly and alignment of nanoparticles in LCs because, in addition to many other reasons, the vacuum levels at which the conventional TEM operates cause LC evaporation. To overcome this problem, and to get insights into the nanoscale structural assembly in nanoparticle-doped LCs, we use a technique known as Freeze Fracture Transmission Electron Microscopy (FFTEM) that has been widely used in the studies of LCs.

The sample preparation for FFTEM imaging starts by taking a small quantity (2–4 μl) of the sample and sandwiching it between two thin copper substrates. This sample between the copper plates is then rapidly quenched in liquid propane to temperatures below −183°C. The copper sandwich is loaded into a BalTec freeze etch machine at a temperature of −140°C and pressure of 10^{-6} mbar. The copper sandwich is then fractured in the cold vacuum. The exposed fractured surfaces are shadowed with ∼2 nm of a platinum-carbon (Pt-C) alloy at 45° and ∼30 nm of carbon normal to the fractured plane. The Pt-C alloy is deposited for image contrast and the layer of carbon is used to improve mechanical stability. The shadowed sample is removed from vacuum, and gradually warmed to room temperature. It is then washed in deionized water, ethanol, and ethyl acetate to remove the LC host and nanoparticles leaving behind Pt-C replicas of the fracture plane. The Pt-C replicas are imaged using the TEM revealing the structural assembly and alignment of nanoparticles in the LC at the fractured plane. We also used an alternative method of FFTEM sample preparation. In this method, a sample of volume ∼2–4 μl is placed in a small copper bowl instead of sandwiching it between two copper plates. The sample in the bowl is frozen and inserted into the freeze etch machine as described above. Fracturing of the frozen sample is then done with a special knife. The rest of the preparation/imaging procedure is the same as described above.

4. Results

4.1. *LC-Nanoparticle Interactions Probed Using Fluorescence*

To explore the basic properties of nano-scale interactions of LC host fluids with nanoparticle inclusions, we use fluorescent Cadmium Selenide Quantum Dots (QDs) [60]. Spatial location of these nanoparticles in the samples can be directly visualized by use of fluorescence signals in fluorescence microscopy or fluorescence

confocal polarizing microscopy. We explore the behavior of nanoparticles as the LC sample is subjected to temperature changes causing phase transitions. To perform these experiments, the dispersion of QDs in hexane is added to a commercial thermotropic nematic mixture E7 (EM Chemicals) at a concentration of 0.001% by weight. The cell with the QD-E7 dispersion is then placed into an Instec STC200 heating stage mounted on a fluorescent microscope. A 10x objective is used with a 488 nm argon laser to obtain monochromatic transmission optical microscopy images between crossed polarizers and corresponding fluorescent images of the sample. The transmission and fluorescence images are overlaid to visualize the nanoparticle spatial locations and interactions (Fig. 4a).

To explore the differences in the behavior of particles in isotropic vs. nematic LC hosts, the temperature to which the sample is subjected in the heating stage is first increased to 80°C and then cooled at 0.5°C/s to room temperature. In the isotropic phase, the QDs are well dispersed and undergo Brownian motion. However, when the LC sample transitions from isotropic to the nematic phase, the QDs are expelled from the nucleated and growing nematic domains into their isotropic surroundings. This expulsion is due to the elastic energy costs associated with the distortions of the LC director by QDs. Retaining QDs in the isotropic phase is energetically favorable because there is no elastic energy cost associated with the isotropic phase while the nanoparticle-induced distortions in the nematic host correspond to the elastic free energy of the order of $KL \geq K_BT$ per nanoparticle, where $K \sim 10$pN is the average Frank elastic constant and L is the average size of nanoparticles. Figure 4a shows a series of images taken as the E7 transitions from isotropic to the nematic phase. The highlighted QDs are expelled from the nematic domain and remain at the

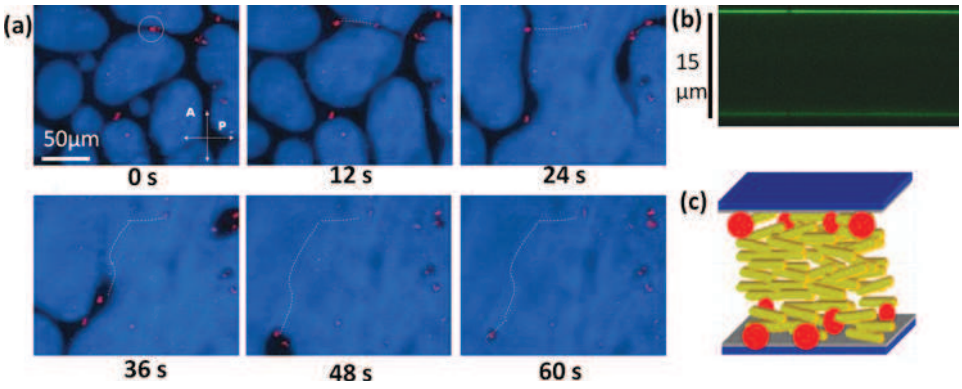

Figure 4. Nanoparticle expulsion from the LC. a) a series of color-coded superimposed images taken in polarizing and fluorescence microscopy modes. The white circle in the image at time $t = 0$ highlights QDs expelled from the LC while remaining in the isotropic melt of the sample until disappearing. The dashed white lines in the images highlights the movement of QDs along about 200 µm-long trajectory across the sample over the course of 1 min. Using Fluoview software of the confocal microscope, the grayscale transmission-mode images with the fluorescence from QDs are color-coded so that the bright areas appear blue, the dark areas appear black, and the strong fluorescence signals from QDs appear red. b) a vertical cross section of nematic LC cell obtained using fluorescence confocal microscopy. Fluorescence from the QD nanoparticles is shown in green. c) a schematic showing QDs expelled to the glass-LC interface. (Figure appears in color online.)

isotopic-nematic phase boundary as long as possible, until the isotropic region of the sample disappears. This expulsion often leads to the transition-induced aggregation of colloidal inclusions. Furthermore, this clearly demonstrates that dispersion of nanoparticles in LC fluids is more challenging as compared to the isotropic solvents and even the nanoparticles that disperse well in isotropic melts of certain materials may aggregate as a result of a transition to the mesophase.

4.2. *Expulsion of Fluorescent Nanoparticles to Confining Substrates*

Partial expulsion of nanoparticles from the LC hosts is also observed for samples deep in the nematic phase. After being kept for several hours in the nematic LC, the fluorescent QDs partially segregate to the nematic-glass interface. The same effect is observed for Quantum Rods (QRs) (Fig. 3g) [43]. Using the dispersion techniques described above, the QRs are dispersed in the nematic mixture ZLI-2806 (obtained from EM Chemicals) at the doping concentration of 0.01% by weight. This nematic has low birefringence, which makes it ideal for imaging by means of a confocal microscope. QRs are excited using a 488 nm Argon laser and imaged using the confocal microscope. Cross sections of the sample are shown in Figure 4b. The fluorescence from the QRs is colored green and can be seen throughout the sample, but is the strongest at the nematic-glass boundary, indicating the segregation of the majority of the nanoparticles onto the substrate. Figure 4c shows a schematic representation of the phase separation. Much like the expulsion of QDs from the nematic nuclei into the surrounding isotropic melt discussed above, the nematic LC expels the distortion-causing QRs to the glass/nematic boundary where this elastic distortion is minimized in size and energy cost. Although this experiment highlights an additional challenge of obtaining long-term-stable nanoparticle dispersions in LCs, it also shows the feasibility of stable dispersion of nanoparticles in the LC as somewhat weaker fluorescent signals also come from the individual QRs in the bulk of the LC which do not segregate (Fig. 4b).

4.3. *Entrapment of Nanoparticles by Defect Networks*

To show that LC defects can be utilized for spatial patterning of nanoparticles, we use a cholesteric LC. Doping the nematic mixture ZLI-4788 with a chiral agent ZLI-811 (both from EM Chemicals) yields a room temperature cholesteric LC with pitch that depends on the amount of the chiral additive. QRs are added to such a mixture with cholesteric pitch of 1 μm at 0.1% concentration by weight. An Olympus BX51 fluorescent microscope is used to obtain epi-fluorescence images as well as transmission-mode polarizing microscopy images. Figure 5a shows the typical oily streak texture of this cholesteric LC when infiltrated into a cell with untreated glass substrates. Figure 5b shows the same area of the sample imaged with fluorescence microscopy. The fluorescence from the QRs is the strongest in the vicinity of oily streaks, indicating that the nanoparticles spatially localize within the defect cores. The self-assembly of the QRs into the defects is driven by the reduction of elastic free energy costs when the nanoparticles are in the defect core as the particles replace energetically costly regions of the defects. Similar to the case of larger colloids [71], the studied QRs stabilize the network of oily streak defects. Since the nanoparticles now tend to stay within the defects, they are less susceptible to segregation to the bounding glass plates.

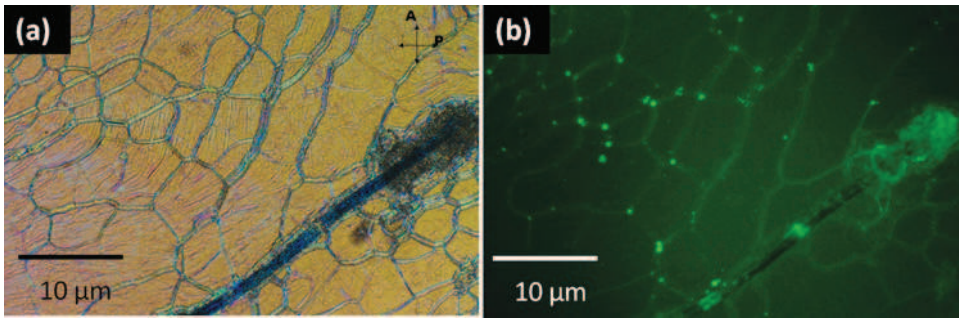

Figure 5. Entrapment of nanoparticles by defects. a) polarizing microscopy image obtained with crossed polarizers showing the cholesteric oily streaks in the planar system of cholesteric layers. b) Fluorescent microscopy images of the LC doped with quantum rods shows that these nanoparticles have self-assembled into the oily streaks making these defects appearing more luminous than the surrounding LC with a uniform cholesteric structure. (Figure appears in color online.)

4.4. *Improving the Stability of Cholesteric Blue Phases Using Nanoparticles*

The feasibility of using periodic networks of defects in blue phases (BPs) as a template for spatial patterning of nanoparticles is explored by use of several different types of nanoparticles and cholesteric TI-827 (from EM Chemicals) with a ~300 nm pitch. Various nanoparticles were added at concentration of ~1% by weight. The doped samples are placed in a heat stage, heated into the isotropic phase and then slowly cooled at 0.1°C/min. To identify the phase of the LC during cooling, transmission-mode polarizing microscopy is employed. Because of the selective reflection of circularly polarized light by cubic phases BPI and BPII, only the circularly polarized light of handedness not reflected by the sample is transmitted and detected by the camera. By analyzing the optical microscopy textures, we measure the overall temperature range of the blue phase existence, i.e., between the transition temperatures from isotropic to cholesteric phases. Table 1 shows that the addition of the nanoparticles increases the overall temperature range of BP stability. This is an indication of nanoparticle self-assembly into defect cores of the disclination network in BPs. The inclusion of nanoparticle also affects the textural appearance of the sample (Fig. 6). Nanoparticles occupying the energetically costly defect cores help to stabilize BPs. Similar to the case of nanoparticles obtained by other means [49], our nanoparticles (synthesized via wet chemical processes) are dispersed and assembled in BPs, showing that the BP-assisted assembly can be achieved for variety of particle

Table 1. Effect of adding nanoparticles on the overall thermal stability range of the cholesteric blue phases of the mesogenic mixture TI-827

Mixture	BP Temperature range,°C
Undopped TI-827	1.5
TI-827 + ~1% CdSe quantum rods (Fig. 3g)	2.4
TI-827 + ~1% thiol-capped nanospheres (Fig. 3a)	2.2
TI-827 + ~1% Nsol nanorods (Fig. 3h)	3.3

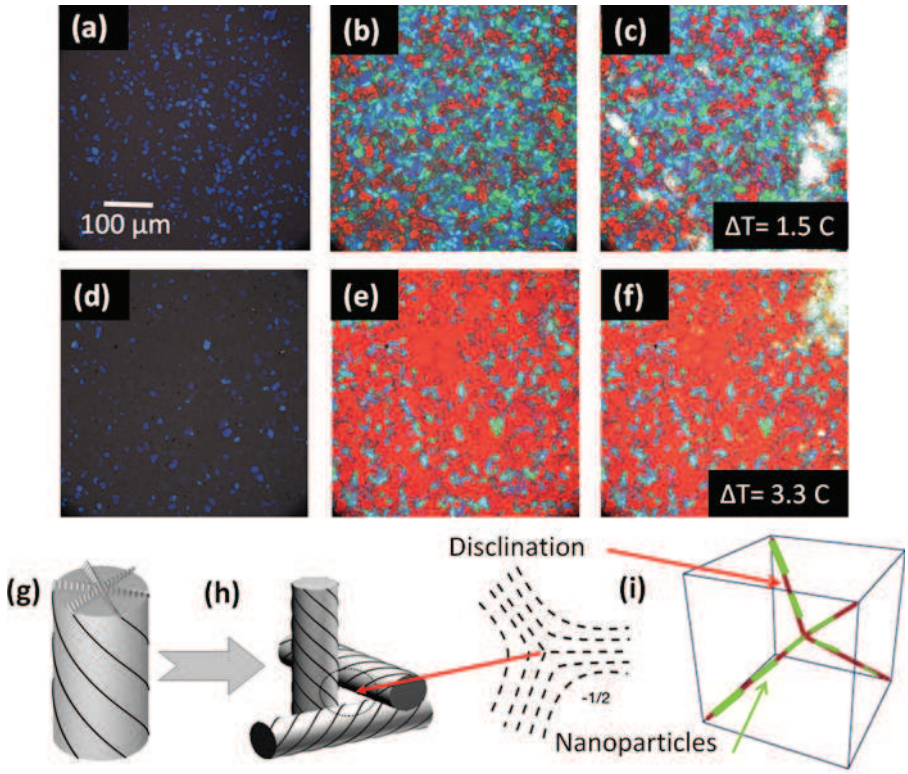

Figure 6. Effect of nanoparticle doping on the stability of the cholesteric blue phase. a-c) the textures of undopped sample cooled from isotropic to cholesteric phase at 0.1C/min. d–f) The textures of nanorod-doped blue phase as the mixture is cooled from isotropic to cholesteric phase at the same rate; the used gold nanorods are shown in Figure 3 h. g) double twist cylinder with the LC molecules aligned along the cylinder axis in its center and twisting in all radial directions when moving away from the center. h) 3D packing of the double twist cylinders into cubic lattices gives rice to disclination defects that form distinct 3D periodic networks in blue phases I and II. i) Nanorods are expected to localize in the defect cores and align along the disclinations. (Figure appears in color online.)

compositions, sizes, and shapes. Since the defect lattices in BPs can have periodicity of 100–200 nm, this spatial patterning is potentially useful for the self-assembly of metamaterials and other novel composite materials.

4.5. *Direct Nanoscale Imaging of Well-Dispersed Nanoparticles in Liquid Crystals*

To demonstrate that certain types of nanoparticles can disperse in the ground-state samples of LCs without aggregating or localizing into defects, we perform FFTEM imaging of the TI-827 doped with gold nanospheres (shown in Fig. 3b) at 10% concentration by weight. Figure 7a,b shows the FFTEM image of the sample having 300 nm pitch with the nanoparticles well-dispersed in the LC, as clearly seen from the high-magnification inset of the same area in the sample. Similar high-quality dispersion of the nanoparticles is seen throughout the sample except in a few areas

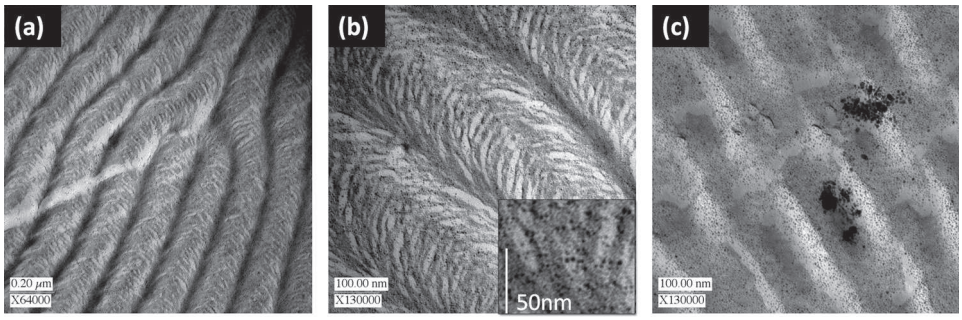

Figure 7. Nanoscale imaging of nanopasrticles dispersed in a cholesteric LC. Freeze fracture TEM images of a) 2–3 nm thiol-capped gold nanospheres dispersed in a short pitch cholesteric and b) a magnified image of (a) showing the high-quality dispersion of the nanoparticles; the inset shows the details of the nanoparticle-doped sample at even higher magnification. c) Local aggregation of nanoparticles seeded by larger nanospheres occasionally present in the sample.

(Fig. 7c) where local aggregation may be ''seeded'' by much larger nanoparticles. The larger nanoparticles create stronger distortions in the LC molecular alignment that may trap surrounding nanoparticles to reduce the elastic distortion costs. Further experiments are needed to investigate how nanoparticle dispersions depend on particle size distribution.

4.6. *Nanoparticle Dispersion, Alignment, and Self-Assembly in Lyotropic Liquid Crystals*

We have previously demonstrated that gold nanorods can be well dispersed and aligned in both nematic and columnar hexagonal lyotropic LCs [15], even at high concentrations when inter-rod distances are comparable to their length. However, other types of behavior of nanorods are possible too, depending on the sizes, shapes, capping of nanorods, as well as the details of their dispersion into the LC hosts. Figure 8 shows FFTEM images obtained for nanorods with length ~400 nm and diameter ~20 nm dispersed in a surfactant-based lyotropic LC similar to that used in our previous studies [15]. Doping these rods (having rather high aspect ratios) into the LC in a columnar hexagonal phase typically causes nano-scale polydomain structure (Fig. 8). By varying the concentration of these nanorods in the LC, we see their periodic self-assembly (Fig. 8b,c), a percolating network of nanorods with a ~200 nm mesh (Fig. 8d,e), and dispersed nanorods aligning along the domain boundaries (Fig. 8f). The observed structures are a result of medium-nanorod interactions minimizing elastic distortions in the nanoparticle-doped LC in the hexagonal phase by eliminating distortions at the nanorod ends (as schematically shown in Fig. 8a) or localizing these nanoparticles within the LC domain boundaries. These observations show a great potential for forming nanoparticle self-assemblies of interest for fabrication of metamaterials and other structured nanocomposites. The addition of these and other nanoparticles to LCs may not only result in their nanoscale self-assembly or simple segregation but also may lead to new complex thermodynamic phases not exhibited by these constituents themselves, such as in the case of lipid-biopolymer composites [72].

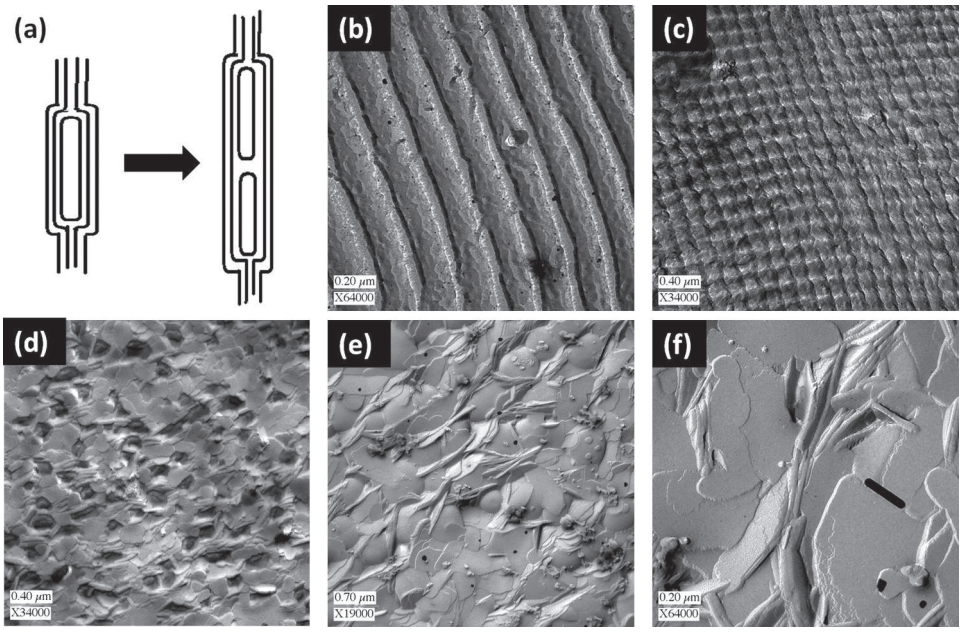

Figure 8. Spatial nanoscale structuring of nanorods dispersed in the 70% water, 25% CTAB, 5% BnOH hexagonal LC hosts. a) Rods in an aligned LC may form chains to reduce elastic energy due to the distortions at their ends. Freeze fracture transmission electron microscopy images of b) long rods forming chains and c) periodic structure in the plane orthogonal to the chains. d,e,f) different 3D networks of nanorods f) aligning along the domain walls between the nanoscale domains in the columnar hexagonal phase of the lyotropic LC.

5. Discussion

Our experimental results presented in this work (and also those published elsewhere [27–31]) show that LC host media allow for multiple ways of structural self-assembly and self-alignment [33] of nanoparticles. However, before the LC media can be used as ''smart'' host fluids for the self-assembly-based fabrication of metamaterials, there is a need for deeper fundamental understanding of the inter-particle forces in LCs and nanoparticle-LC interactions as well as finding ways of dealing with numerous technical challenges. One of the main challenges is the robust stabilization of colloidal nano-scale dispersions in various LC phases. Figure 4 shows that even nanoparticles that are well dispersed in the isotropic phase of LC can aggregate and be expelled out due to their interactions with the host fluid once it transitions into the ordered viscoelastic LC phase. This expulsion from a host fluid in the nematic phase is caused by the elastic free energy cost of the nanoscale director distortions introduced by the inclusion. Expulsion of a nanoparticle into the isotropic melt (Fig. 4a) of the LC reduces the overall free energy by the energy cost of distortions, typically of the order of KL, where K is the average elastic constant and L is the average size of the inclusion. When the nanoparticles are expelled to surfaces (Fig. 4b,c), one obtains a similar reduction of the elastic energy as the nanoparticle-induced distortions partially disappear while the colloids localize at the surfaces.

The enhanced aggregation of nanoparticles in the LC hosts is often facilitated by the elasticity-mediated inter-nanoparticle interactions. Studies of colloidal micro-particles in nematic LCs reveal strongly anisotropic long-range interactions that can be of both attractive and repulsive nature [73,74]. These interactions typically depend on topological defects and director distortions occurring around the particles and are mediated by orientational elasticity of the surrounding LC. In the case of micron-sized inclusions embedded in a nematic LC, both dipolar and quadrupolar configurations can occur, depending on the surface anchoring. When the orientation of the "easy axis" of the director is normal to the surface of the particle, linear colloidal chains are typically formed owing to the long-range dipolar attraction between elastic dipoles formed by particles and hyperbolic point defects. The short range repulsive interactions associated with the presence of the hyperbolic point defects close to the colloids prevent aggregation. When the surface anchoring at the LC-colloid interface is weak-vertical or planar, more complex structures form due to director distortions of quadrupolar symmetry, such as the ones involving Saturn ring disclinations or surface point defects called boojums [28]. These interactions often result in aggregation of particles into chains at a certain angle with respect to the far-field LC director. When the particle size is $\sim$50 nm or smaller, their size is comparable or smaller than the typical surface anchoring extrapolation length for the case of strong surface boundary conditions, and all spherical particles induce director distortions of quadrupolar symmetry; thus, elasticity mediated forces in anisotropic fluids like nematics may facilitate their irreversible anisotropic aggregation. This suggests several approaches for overcoming the problems of irreversible aggregation discussed below.

One approach is to impose strong vertical boundary conditions or use particles of low-symmetry shapes so that dipolar rather than quadrupolar director distortions form around the LC colloids [31]. Relatively large nanoparticles ($\sim$50 nm and larger) or nanoparticles of well-controlled specific shapes can be stabilized using this method. The other approach is to use LCs with partial positional ordering, such as smectic and columnar LCs, as successfully realized in our previous works [15,29,30]. The layered or columnar structures with one-dimensional or two-dimensional positional ordering, respectively, restrict particle motion to the directions in which the LC is fluid and the nanoparticles can then be stabilized even by use of the very same elasticity-mediated quadrupolar interactions that can be repulsive in the directions in which colloids are allowed to move [15,29,30]. Yet another approach is to make the inter-particle interactions sufficiently weak and comparable in strength to that of thermal fluctuations. In this case, the particles properly stabilized in isotropic melt of the thermotropic LC or in the dilute aqueous solutions will be also stable in the thermotropic or lyotropic mesophases, respectively. Figure 7 demonstrates how this is achieved for small nanoparticles of size $\sim$2 nm in the same cholesteric LC in which larger particles aggregate. The smaller nanoparticles are well dispersed because, due to their size, they barely perturb the ground-state LC structure and the elastic energy cost of the surrounding distortions is negligible or comparable to the thermal energy. Increasing the size of similar particles to 10–15 nm already makes them unstable as the cost of elastic energy distortions increases with the particle size. Particles of larger size can be stabilized in lyotropic nematic LCs made of cylindrical micelles [15] due to the fact that elastic constants of these LCs are about an order of magnitude smaller than in the case of thermotropic LCs. Interestingly, even in the cases when the elasticity-mediated

interactions are weak, nanoparticle orientation with respect to the LC director can be controlled and depends on the symmetry of nanoparticle shape, its surface treatment, and the mesophase of the LC host [15,31].

The very same nanoparticle-induced elastic distortions that make their colloidal stabilization more difficult compared to that in isotropic fluids can be utilized for the controlled spatial patterning of nanoparticles. The nanoinclusion-induced distortions give rise to the elasticity-mediated interactions of the particles with defects and other distortions that can be deliberately induced by external fields and beams of light or pre-defined by ground states of certain phases, such as blue phases. The oily streak defects in the cholesteric phase, for example, attract the surrounding CdSe nanoparticles (Fig. 5), so that the defects in the doped samples strongly fluoresce, giving direct evidence for the location of particles in the defect cores (with the majority being concentrated in the defect nodes). Because of the existing network of defect lines in BPs, the nanorods can spatially localize into the defect cores, thus reducing the overall free energy by eliminating the energetically-costly regions of the disclination cores and sharing the distortions around nanorods with those due to defects. This not only allows for the nanoscale positioning of nanoparticles into the periodic three-dimensional network of defects cores but also for another practically useful effect, the increase of the temperature range of the BP existence (Table 1). Similar stabilization effect has been observed for various other types of nanoparticles, both experimentally and theoretically [49,75,76], showing that nanoparticle-doped cholesteric BPs emerge as a class of composites of interest for applications.

In addition to the spatial localization and patterning of nanoparticles, we have recently demonstrated aggregation-free elastic self-alignment of nanorods dispersed in LCs and their realignment by shearing and magnetic fields [15]. The orientational self-ordering of gold nanorods is a result of the elastic interaction of nanorods with the surrounding matrix of a uniformly aligned LC. The elastic energy is minimized for the nanorod alignment parallel to the far-field director because the elastic distortions in this case occur only at the rod ends. In the case of gold nanorods, this self-alignment gives rise to the strong polarization sensitivity of SPR, showing the potential for LC-mediated oriented self-assembly of bulk optical metamaterials with tunable and switchable properties [15]. External magnetic/electric fields and shearing allow for alignment and realignment of the LC matrix with the ensuing reconfigurable long-range orientational order of the dispersed nanoparticles that can be kept well dispersed during this process. A number of interesting structures can be achieved as a result of elasticity-mediated spatial patterning of nanoparticles in different LCs, ranging from the aligned nematic-like arrangements of well-dispersed nanorods [15] to translationally periodic chains and arrays of nanorods, and to the percolating three-dimensional network of these nanoparticles (Fig. 8). The experiments show a very broad spectrum of self-assembly phenomena that depend on the size and shape of nanoparticles, the type of LC used, etc. For example, the formation of long periodically-spaced chains shown in Figure 8b allows the elimination of the strong elastic distortions induced at the opposite particle ends or share some of the distortions (Fig. 8a). Clearly, the long nanorods show a distinctly different behavior as compared to the case of short nanorods and either assemble into long chains or cause a nanoscale polydomain structure of the surrounding lyotropic LC and segregate into the domain walls, forming a three-dimensional percolating network of nanorods in the LCs.

6. Conclusions

In conclusion, we have demonstrated dispersion, self-alignment, and self-assembly of plasmonic metal nanoparticles in liquid crystals. Since the LC-mediated alignment and assembly of plasmonic nanoparticles gives rise to a switchable polarization-sensitive plasmon resonance (exhibiting stark differences from that of the same nanoparticles in isotropic fluids [15]), the LCs with self-assembled and self-aligned anisotropic nanoparticles are of interest for fabrication of tunable optical metamaterials. Furthermore, once the understanding and control of the underlying physical processes are improved, the device-scale bulk nanoparticle self-alignment and self-assembly may enable optical metamaterial mass production and control of their properties arising from combining the switchable nanoscale structure of LCs and the surface plasmon resonance properties of the plasmonic nanopartricles.

Acknowledgment

This work was supported by the Renewable and Sustainable Energy Initiative and Innovation Initiative Seed Grant Programs of University of Colorado at Boulder, International Institute for Complex Adaptive Matter, and by NSF grants DMR0645461, HRD0639653, DMR0820579, and DMR0847782. D.G. was supported by the SMART undergraduate research program of the Colorado Diversity Initiative. We thank Paras Prasad and Ken-Tye Yong for providing quantum dots and rods used in our studies. We thank Richard Gursky for discussions and for his help with obtaining the cryogenic TEM images of the chromonic LC samples. We also thank Corinne Beier, Budhadipta Dan, Clayton Lapointe, Qingkun Liu, Angel Martinez, Hector Mireles, Ramarao Pratibha, Sabrina Thompson, Rahul Trivedi, Christopher Twombly, and Bethany Wilcox for discussions and various assistance at different stages of this project.

References

[1] Veselago, V. G. (1968). *Soviet Physics Uspekhi*, *10*, 509.
[2] Pendry, J. B. (2000). *Phys Rev. Lett.*, *85*, 3966.
[3] Werner, D. H., Kwon, D. H., Khoo, I. C., Kildishev, A. V., & Shalaev, V. M. (2007). *Optics Express*, *15*, 3342.
[4] Minovich, A., Neshev, D. N., Powell, D. A., Shadrivov, I. V., & Kivshar, Y. S. (2010). *Appl. Phys. Lett.*, *96*, 193103.
[5] Soukoulis, C. M., Linden, S., & Wegener, M. (2007). *Science*, *315*, 47.
[6] Li, T., Li, Y. Q., Wang, F. U., Wang, Q. J., Liu, H., Zhu, S. N., & Zhu, Y. Y. (2007). *Appl. Phys. Lett.*, *90*, 251112.
[7] Valentine, J., Zhang, S., Zentgraf, T., Ulin-Avila, E., Genov, D., Bartal, G., & Zhang, X. (2008). *Nature*, *455*, 376.
[8] Kim, E., Wang, F., Wu, W., Yu, Z., & Shen, Y. R. (2008). *Phys. Rev. B.*, *78*, 113102.
[9] Minovich, A., Neshev, D. N., Powell, D. A., Shadrivov, I. V., Lapine, M., McKerracher, I., Hattori, H. T., Tan, H. H., Jagadish, C., & Kivshar, Y. S. (2010). *Phys, Rev. B.*, *81*, 115109.
[10] Zhang, S., Fan, W., Panoiu, N. C., Malloy, K. J., Osgood, R. M., & Brueck, S. R. J. (2005). *Phys. Rev. Lett.*, *95*, 1347404.
[11] Dolling, G., Enkrich, C., Wegener, M., Soukoulis, C. M., & Linden, S. (2006). *Science*, *312*, 892.

[12] Wu, W., Kim, E., Ponizovskaya, E., Liu, Y., Yu, Z., Fang, N., Shen, Y. R., Bratkovsky, A. M., Tong, W., Sun, C., Zhang, X., Wang, S. Y., & William, R. S. (2007). *Appl. Phys A: Matter. Sci. Process.*, *87*, 143.
[13] Chettiar, U. K., Kildishev, A. V., Yuan, H. K., Cai, W., Xiao, S., Drachev, V. P., & Shalaev, V. M. (2007). *Optics Lett.*, *32*, 1671.
[14] Plum, E., Zhou, J., Dong, J., Fedotov, V. A., Koschny, T., Soukoulis, C. M., & Zheludev, N. I. (2009). *Phys. Rev. B*, *79*, 03540.
[15] Liu, Q., Cui, Y., Gardner, D., Li, X., He, S., & Smalyukh, I. I. (2010). *Nano Lett*, *10*, 1347.
[16] Yao, J., Liu, Z., Liu, Y., Wang, Y., Sun, C., Bartal, G., Stacy, A. M., & Zhang, X. X. (2008). *Science*, *321*, 930.
[17] Khoo, I. C., Werner, D. H., Liang, X., & Diaz, A. (2006). *Optics Lett.*, *31*, 2592.
[18] Zhang, S., Park, Y. S., Li, J., Lu, X., Zhang, W., & Zhang, X. (2009). *Phys. Rev. Lett.*, *102*, 023901.
[19] Podolskiy, V. A., Sarychev, A. K., & Shalaev, V. M. (2002). *J. Nonlinear Optical Phys. and Mater. Sci.*, *11*, 65.
[20] Podolskiy, V., Sarychev, A., & Shalaev, V. (2003). *Optics Express*, *11*, 735.
[21] Shalaev, V., Cai, W., Cettiar, U. K., Yuan, H. K., Sarychev, A. K., Drachev, V. P., & Kildishev, A. V. (2005). *Optics Lett.*, *30*, 3356.
[22] Linden, S., Enkrich, C., Wegener, M., Zhou, J., Koschny, T., & Soukoulis, C. M. (2004). *Science*, *306*, 1351.
[23] Zhang, S., Fan, W., Minhas, B. K., Frauenglass, A., Malloy, K. J., & Brueck, S. R. J. (2005). *Phys. Rev. Lett.*, *94*, 037402.
[24] Smith, D. R., Padilla, W. J., Vier, D. C., & Nemat-Nasser, S. C., & Schultz, S. (2000). *Phys. Rev. Lett.*, *84*, 4184.
[25] Baena, J. D., Jelinek, L., & Marques, R. (2007). *Phys. Rev. B*, *76*, 245115.
[26] Liu, N., Liu, H., Zhu, S., & Giessen, H. (2009). *Nature Photonics*, *3*, 157.
[27] Lapointe, C., Hopkins, S., Mason, T. G., & Smalyukh, I. I. (2010). *Phys. Rev. Lett.*, *105*, 178301.
[28] Smalyukh, I. I. (2010). *Proc. Nat. Acad. U.S.A.*, *107*, 3945.
[29] Pratibha, R., Park, W., & Smalyukh, I. I. (2010). *J. Appl. Phys.*, *107*, 063511.
[30] Pratibha, R., Park, K., Smalyukh, I. I., & Park, W. (2009). *Optics Express*, *17*, 19459.
[31] Lapointe, C., Mason, T., & Smalyukh, I. I. (2009). *Science*, *326*, 1083.
[32] Khoo, I. C., Werner, D. H., Liang, X., & Diaz, A. (2006). *Optics Lett.*, *31*, 2592.
[33] Stebe, K. J., Lewandowski, E., & Ghosh, M. (2009). *Science*, *325*, 159.
[34] Swami, A., Selvakannan, P. R., Pasricha, R., & Sastry, M. (2004). *J. Phys. Chem. B.*, *108*, 19269.
[35] Fukuto, M., Heilmann, R. K., Pershan, P. S., Badia, A., & Lennox, R. B. (2004). *J. Chem. Phys.*, *120*, 3446.
[36] Shenhar, R., Norsten, T. B., & Rotello, V. M. (2005). *Advanced Materials*, *17*, 657.
[37] Perez-Juste, J., Rodrigues-Gonzalez, B., Mulvaney, P., & Liz-Marzan, L. (2005). *Adv. Funct. Mater.*, *15*, 1065.
[38] Elghanian, R., J.Storhoff, J., Mucic, R. C., Letsinger, R. L., & Mirkin, C. A. (1997). *Science*, *277*, 1078.
[39] Hegmann, T., Qi, H., & Marx, V. M. (2007). *J. Inorg. Organomet. Polym. Mater.*, *17*, 483.
[40] Perez-Juste, J., Liz-Marzan, L. M., Carnie, S., Chan, D. Y. C., & Mulvaney, P. (2004). *Adv. Funct. Mater.*, *14*, 571.
[41] Lynch, M. D., & Patrick, D. L. (2002). *Nano Lett.*, *2*, 1197.
[42] Baker, J. L., Widmer-Cooper, A., Toney, M. F., Geissler, P. L., & Alivisatos, A. P. (2010). *Nano Lett.*, *10*, 195.
[43] Sonnichsen, C., & Alivisatos, A. P. (2005). *Nano Lett.*, *5*, 301.
[44] Ahmed, W., Kooij, E. S., & van Silfhout, A., & Poelsema, B. (2009). *Nano Lett.*, *9*, 3786.

[45] Zhang, S., Leem, G., Srisombat, L., & Lee, T. R. (2008). *J. Am. Chem. Soc.*, *130*, 113.
[46] Halle, B., Quist, P. O., & Furó, I. (1992). *Phys. Rev. A*, *45*, 3763.
[47] Wu, K. J., Chu, K. C., Chao, C. Y., Chen, Y. F., Lai, C. W., Kang, C. C., Chen, C. Y., & Chou, P. T. (2007). *Nano Lett.*, *7*, 1908.
[48] Yong, K. T., Sahoo, Y., Swihart, M., & Prasad, P. (2006). *Advanced Materials*, *18*, 1978.
[49] Yoshida, H., Tanaka, Y., Kawamoto, K., Kubo, H., Tsuda, T., Fujii, A., Kuwabata, S., Kikuchi, H., & Ozaki, M. (2009). *Applied Physics Express*, *2*, 121501.
[50] Lydon, J. (1998). *Current Opin. Colloid & Interface Sci.*, *3*, 458.
[51] Kachynski, A. V., Kuzmin, A. N., Prasad, P. N., & Smalyukh, I. I. (2008). *Optics Express*, *16*, 10617.
[52] Kachynskii, A., Kuzmin, A., Prasad, P. N., & Smalyukh, I. I. (2007). *Appl. Phys. Lett.*, *91*, 151905.
[53] Smalyukh, I. I., Kaputa, D., Kachynski, A. V., Kuzmin, A. N., & Prasad, P. N. (2007). *Optics Express*, *15*, 4359.
[54] Salter, P. S., Carbone, G., Botcherby, E. J., Wilson, T., Elston, S. J., & Raynes, E. P., E. P. (2009). *Phys, Rev. Lett.*, *103*, 257803.
[55] Smalyukh, I. I., Shiyanovskii, S., & Lavrentovich, O. D. (2001). *Chem. Phys. Lett.*, *336*, 88–96.
[56] Lee, T., Trivedi, R. P., & Smalyukh, I. I. (2010). *Opt. Lett.*, *35*, 3447.
[57] Xie, A., & Higgins, D. A. (2004). *Appl. Phys. Lett.*, *84*, 4014.
[58] Rust, M. J., Bates, M., & Zhuang, X. (2006). *Nature Methods*, *3*, 793.
[59] Betzig, E., Patterson, G. H., Sougrat, R., Lindwasser, O. W., Olenych, S., Bonifacino, J. S., Davidson, M. W., Lippincott-Schwartz, J., & Hess, H. F. (2006). *Science*, *313*, 1642.
[60] Prasad, P. N. (2004). *Nanophotonics*. Wiley: Hoboken, US.
[61] Grzelezak, M., Juste, J., Mulvaney, P., & Liz-Marzan, L. (2008). *Chem. Soc. Rev.*, *37*, 1783.
[62] Brust, M., Walker, M., Bethell, D., Schiffrin, D., & Whyman, R. J. (1994). *J. Chem. Soc., Chem. Commun.*, 801.
[63] Murphy, C., Sau, T., Gole, A., Orendorff, C., Gao, J., Gou, L., Hunyadi, S., & Li, T. J. (2005). *Phys. Chem. B*, *109*, 13857.
[64] Wang, C., Wang, T., Ma, Z., & Su, Z. (2005). *Nanotechnology*, *16*, 2555.
[65] Jana, N. R., Gearheart, L., & Murphy, C. J. (2001). *Langmuir*, *17*, 6782.
[66] Nikoobakht, B., & El-Sayed, M. A. (2003). *Chem. Mater.*, *15*, 1957.
[67] Pietrobon, B., & Kitaev, V. (2008). *Chemistry of Materials*, *20*, 5186.
[68] Chandran, S., Chaudhary, M., Pasricha, R., Ahmad, A., & Sastry, M. (2006). *Biotechnol Prog.*, *22*, 577.
[69] Clawson, J. S., Holland, G. P., & Alam, T. M. (2006). *Phys. Chem. Chem. Phys.*, *8*, 2635.
[70] Montalvo, G., Valiente, M., & Todenas, E. J. (1995). *Colloid Interface Sci.*, *172*, 494.
[71] Zapotocky, M., Ramos, L., Poulin, P., Lubensky, T. C., & Weitz, D. A. (1999). *Science*, *283*, 209.
[72] Koltover, I., Salditt, T., Radler, J. O., & Safinya, C. R. (1998). *Science*, *281*, 78.
[73] Poulin, P., Stark, H., Lubensky, T. C., & Weitz, D. A. (1997). *Science*, *275*, 1770.
[74] Lubensky, T. C., Pettey, D., Currier, N., & Stark, H. (1998). *Phys. Rev. E*, *57*, 610.
[75] Karatairi, E., Rožič, B., Kutnjak, Z., Tzitzios, V., Nounesis, G. Cordoyiannis, G., Thoen, J., Glorieux, C., & Kralj, S. (2010). *Phys. Rev. E*, *81*, 041703.
[76] Kikuchi, H., Yokota, M., Hisakado, Y., Yang, H., & Kajiyama, T. (2002). *Nature Mater.*, *1*, 64.